Corrected: Author Correction

Emerging photoluminescence from the dark-exciton phonon replica in monolayer WSe$_2$

Zhipeng Li [1,2,13], Tianmeng Wang[1,13], Chenhao Jin [3,13], Zhengguang Lu[4,5], Zhen Lian[1], Yuze Meng[1,6], Mark Blei[7], Shiyuan Gao[8], Takashi Taniguchi[9], Kenji Watanabe [9], Tianhui Ren[2], Sefaattin Tongay[7], Li Yang[8], Dmitry Smirnov [4], Ting Cao[10,11] & Su-Fei Shi [1,12]

Tungsten-based monolayer transition metal dichalcogenides host a long-lived "dark" exciton, an electron-hole pair in a spin-triplet configuration. The long lifetime and unique spin properties of the dark exciton provide exciting opportunities to explore light-matter interactions beyond electric dipole transitions. Here we demonstrate that the coupling of the dark exciton and an optically silent chiral phonon enables the intrinsic photoluminescence of the dark-exciton replica in monolayer WSe$_2$. Gate and magnetic-field dependent PL measurements unveil a circularly-polarized replica peak located below the dark exciton by 21.6 meV, equal to E″ phonon energy from Se vibrations. First-principles calculations show that the exciton-phonon interaction selectively couples the spin-forbidden dark exciton to the intra-valley spin-allowed bright exciton, permitting the simultaneous emission of a chiral phonon and a circularly-polarized photon. Our discovery and understanding of the phonon replica reveals a chirality dictated emission channel of the phonons and photons, unveiling a new route of manipulating valley-spin.

[1] Department of Chemical and Biological Engineering, Rensselaer Polytechnic Institute, Troy, NY 12180, USA. [2] School of Chemistry and Chemical Engineering, Shanghai Jiao Tong University, 200240 Shanghai, China. [3] Kavli Institute at Cornell for Nanoscale Science, Ithaca, NY 14853, USA. [4] National High Magnetic Field Lab, Tallahassee, FL 32310, USA. [5] Department of Physics, Florida State University, Tallahassee, FL 32306, USA. [6] College of Physics, Nanjing University, 210093 Nanjing, China. [7] School for Engineering of Matter, Transport and Energy, Arizona State University, Tempe, AZ 85287, USA. [8] Department of Physics, Washington University in St. Louis, St. Louis, MO 63136, USA. [9] National Institute for Materials Science, 1-1 Namiki, Tsukuba 305-0044, Japan. [10] Geballe Laboratory for Advanced Materials, Stanford University, Stanford, CA 94305, USA. [11] Department of Materials Science and Engineering, University of Washington, Seattle, WA 98195, USA. [12] Department of Electrical, Computer & Systems Engineering, Rensselaer Polytechnic Institute, Troy, NY 12180, USA. [13] These authors contributed equally: Zhipeng Li, Tianmeng Wang, Chenhao Jin. Correspondence and requests for materials should be addressed to T.R. (email: thren@sjtu.edu.cn) or to T.C. (email: tingcao@uw.edu) or to S.-F.S. (email: shis2@rpi.edu)

Light-matter interactions are often dictated by optical selection rules that enable access to unique material properties such as valley-spin degrees of freedom in transition metal dichalcogenides (TMDCs)[1–10]. However, the selection rules based on electric dipole approximations also render many important processes optically "dark", prohibiting the extraction of critical material properties. To overcome this limitation, careful maneuvering of the selection rules through higher order interactions provides access to the otherwise dark states and reveal additional rich physics. To this end, two-photon luminescence spectrum probes the 2p exciton states of carbon nanotube[11] and WS₂[12], which provides critical information about the exciton binding energies[13–17]. Raman spectroscopy reveals the 2D vibration mode of graphene through two-phonon process, which played a significant role in identifying graphene layer number in the early stage of graphene research[18,19].

In this letter, we report the emerging circularly polarized photoluminescence of dark-exciton phonon replica states in monolayer WSe₂, which arises from a second-order interaction between the spin-forbidden dark exciton and the phonon-photon degree of freedom, providing a completely new strategy to investigate the exciton-spin manifold. The chiral E″-phonon-assisted interaction[20–26] between the dark exciton and light leads to circularly polarized photoluminescence (PL) from the phonon-replica state, which we unambiguously reveal and identify by the magnetic field- and gate-dependent PL spectroscopies. The energy of the E″ phonon mode is extracted experimentally to be 21.6 meV, which is in excellent agreement with the E″ phonon mode from first-principles calculations (21.8 meV; see Supplementary Note 13). We further provide a microscopic model and demonstrate the brightening of the dark exciton state through the unique role of the phonon mode, which acts as a fluctuating in-plane effective magnetic field and mixes the spin-allowed (bright) and spin-forbidden (dark) exciton states of the same valley. Our observation, therefore, opens up exciting new possibilities to probe and control the dark exciton state on its light-interaction, spin properties, and dynamics.

Results

Emergence of the dark-exciton replica in monolayer WSe₂.
We fabricate the BN/WSe₂/BN van der Waals (vdW) heterostructure through a dry pickup method which avoids exposing any vdW interface to polymer[27–29]. Two pieces of few-layer graphene were used as the contact electrode to monolayer WSe₂ and the transparent top gate electrode, respectively, with the top BN layer working as the dielectric. A schematic representation of the device is shown in Fig. 1a. With the continuous wave (CW) laser excitation centered at 1.879 eV and a low excitation power of 60 μW, low temperature (4.2 K) PL spectra of the device shown in Fig. 1b resolve distinct peaks from different excitonic complexes, including the dark exciton[30–34]. The presence of the dark exciton arises from the unique band structure of monolayer WSe₂, in which the conduction band minimum and valence band maximum are opposite in spin orientations and the lowest-energy electron-hole pairs form spin-forbidden excitons (Fig. 1d). As a result, light emission with an in-plane electric dipole is strictly forbidden, and an in-plane magnetic field[30] or the coupling to a plasmonic structure[32] is required to brighten the dark exciton. However, using an objective of large numerical aperture (N.A.), the PL of the dark exciton can still be directly observed in high-quality samples, since the radiation from a small out-of-plane dipole[33] of the dark exciton can be collected by the objective. In this case, a well-resolved dark exciton PL peak appears with a narrow linewidth. We perform valley-resolved PL spectroscopy on our devices using optical excitation with certain circular

polarization (σ^+ or σ^-), and detect the PL of the same or opposite circular polarization[1,2,4,8,35–38]. Such a configuration of excitation and detection is labeled ($\sigma^\pm,\sigma^\pm$) in our work. Without applying a top gate voltage and magnetic field, the circularly polarized PL spectra in the (σ^-,σ^-) configuration clearly resolve the charge-neutral exciton X_0 and two well-separated negative trions[38–41], X_1^- and X_2^-, indicative of an initially lightly electron-doped sample. The linewidths of the two trions are 2.1 and 2.2 meV, respectively, much smaller than their energy splitting of ~7 meV[30,38–40,42–45]. It is worth noting that the linewidth of the dark exciton is as narrow as 0.9 meV, which demonstrates the quality of the spectra and is the key to our discovery of the dark-exciton replica. With the application of an out-of-plane magnetic field of 6 T, the exciton (X_0), trion 1 (X_1^-), and trion 2 (X_2^-) peaks all are blue shift in energy and remain a single peak in the PL spectra (magenta curve in Fig. 1b), indicating that their emission is intrinsically circularly polarized at each valley. However, the dark exciton PL at 1.689 eV splits into two peaks at 1.687 and 1.690 eV at 6 T. This splitting occurs because the small out-of-plane electric dipole of dark excitons is expected to result in linearly polarized rather than circularly polarized light for each wave-vector. Therefore, the emissions from the two valleys could both be detected in this σ^- collection configuration, with their energy difference dictated by the valley Zeeman effect[45–48]. Remarkably, another PL peak (indicated by arrows in Fig. 1b) emerges and exhibits behavior similar to the dark excitons. This PL peak, located at 1.667 eV, splits into two peaks with unequal heights at 1.665 and 1.669 eV, with the application of the magnetic field of 6 T. For this reason, we label this peak as the dark-exciton replica (X_D^R). We have reproduced X_D^R in four different BN encapsulated WSe₂ devices (see Supplementary Notes 7 and 8). The power-dependent PL intensity of the exciton, dark exciton, and dark exciton replica is shown in Fig. 1d (solid dots) at the absence of the magnetic field. The PL intensity can be fitted with a power law: $I \sim P^a$, where I is the PL intensity and P is the excitation laser power. It is evident that the dark exciton replica and dark exciton share similar power-law exponent, different from that of the bright exciton (X_0). With low excitation power ($P \leq 40$ μW), the α values are 1.19 and 1.24 for the dark exciton and dark exciton replica, respectively. With higher excitation power, saturation behavior starts to occur and the α values are 0.72 and 0.77 for the dark exciton and dark exciton replica, respectively. In comparison, the PL-power scaling for the bright exciton (X_0) can be described with an α value of 1.13 throughout the whole excitation power range studied. The slight super-linear behavior of the excitation power dependence for the bright exciton (X_0) is consistent with previous reports[28,30].

Magneto-PL spectra of WSe₂.
The connection between X_D^R and X_D can also be revealed through circularly polarized magneto-PL spectra measurements taken in the (σ^-,σ^-) configuration (Fig. 2). We note that the intensity oscillation as a function of the B field is a measurement artifact, which we attribute to the slight beam position shift as we increase the magnetic field. As shown in Fig. 2a, it is evident that all the peaks, except for X_D and X_D^R, undergo a monotonic blue-shift as a function of the out-of-plane magnetic field due to the valley Zeeman effect[45–48]. On the contrary, X_D and X_D^R exhibit a splitting that increases linearly with the magnetic field. The emission energy in the presence of the magnetic field can be expressed as $E = E_0 \pm \frac{1}{2}g\mu_B B$, where g is the Landé g-factor of the excitonic complex of interest, μ_B the Bohr magneton. "+" and "−" correspond to the PL peak energies from the K and K' valleys, respectively. For the bright exciton, only K' valley radiation (σ^-) is allowed to be detected in the valley polarized PL spectra of the (σ^-,σ^-) configuration, and hence, only
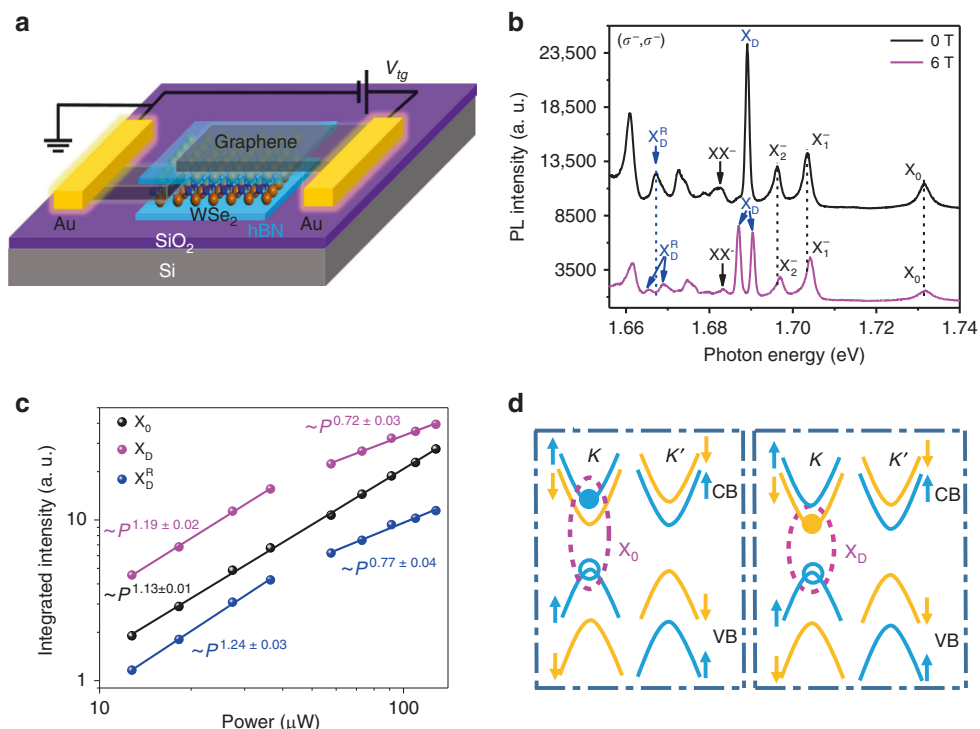
Fig. 1 Dark exciton PL splitting in magnetic field. **a** Schematic representation of BN encapsulated monolayer WSe_2 with graphene contact and top gate electrodes. **b** PL spectra of the device in (**a**) at 4.2 K without the application of the top gate voltage, with no magnetic field (black) and with 6 T out-of-plane magnetic field (magenta) applied. **c** Integrated PL intensity of WSe_2 as a function of the excitation power for the X_0, X_D and X_D^R PL peaks. **d** Schematic configurations of exciton and dark-exciton states with the solid and empty dots representing the electron and hole. Blue and orange colors stand for spin-up and spin-down bands, respectively
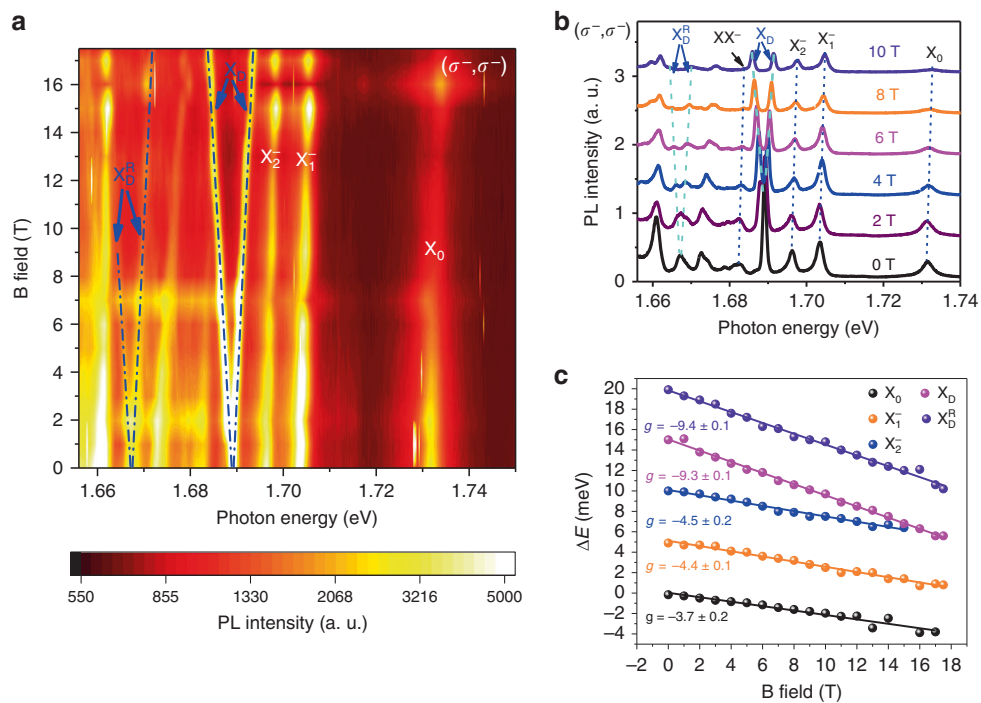
Fig. 2 Valley-resolved magneto-PL spectra of the dark-exciton and its replica. **a** Valley-resolved PL spectra at 4.2 K as a function of the emission photon energy and the applied out-of-plane magnetic field, with the excitation of a CW laser centered at 1.879 eV and excitation power of 60 μW. The color represents the PL intensity. The dark exciton and its replica exhibit distinctively different magnetic field dependence compared to bright excitonic complexes. **b** Line traces of the PL spectra as a function of the applied magnetic field. The dashed lines are the guide for the eye. **c** g-factor for different excitonic complexes obtained from the Zeeman splitting between the E^K and $E^{K'}$, obtained from (**a**) and Supplementary Fig. 5c. The data sets are offset 5 meV intentionally in y-axis for clarity

the blue-shifted emission is observed. The Zeeman splitting between the two valleys, $\Delta E = E^K - E^{K'} = g\mu_B B$, is plotted in Fig. 2c (dots) where g-factor can be obtained through a linear fitting (solid lines). The g-factor for the bright exciton, trion X_1^-, and trion X_2^- are -3.7, -4.4, and -4.5, respectively, consistent with previous studies[28,43,44,49] and a theoretical expectation of -4 based on a noninteracting particle analysis (see Supplementary Note 3). The g-factor for the dark exciton, however, is -9.3, consistent with previous reports[28,31,49] and the theoretical expectation of -8 (see Supplementary Note 3). Interestingly, the dark exciton replica X_D^R has a g-factor of -9.4, similar to that of the dark exciton X_D but distinctly different from those of the bright exciton and trions. This particular magnetic field dependence of X_D^R indicates that its spin-valley configuration is almost identical to that of the dark exciton X_D (see Supplementary Note 7). It is worth noting that the relative intensity of the two branches of the dark exciton replica in the magneto-PL spectra sensitively depends on the circular polarization of bright exciton in the (σ^+, σ^+) or (σ^-, σ^-) measurement (Fig. 2a). The high-intensity branch switches as the helicity of circularly polarized excitation switch (see Supplementary Fig. 5e, f) as it closely follows the Zeeman-shifted circularly polarized bright exciton. This is in stark contrast to the two branches of the dark exciton, which are always the same in intensity regardless of the helicity of the detection. The close correlation of the high PL intensity branch of the dark exciton replica and the bright exciton strongly supports our theory of the phonon-mediated mixing of the dark exciton and bright exciton. The slight difference between the valley polarization of the dark exciton replica and the bright exciton at finite magnetic field can be potentially attributed to the higher order mixing process, which is beyond the scope of this work.

Gate-voltage-dependent PL of WSe₂. To further explore the origin of the replica, we investigate the PL spectra as a function of the top gate voltage for a second device, and the results are shown in Fig. 3. (The gate dependence of device 1, shown in Figs. 1 and 2, is included in Supplementary Note 8.) We employ a CW laser centered at 1.959 eV with an excitation power of 40 μW, under which the biexciton (XX) and negatively charged biexciton (XX⁻) can both be observed[28]. The X_D^R peak of the second device is located at 1.676 eV, slightly higher in energy than the X_D^R peak (1.667 eV) in the first device. Despite the small peak-energy shift, which possibly arises from the residual strain, the splitting between the X_D^R and X_D in the second device remains almost the same as that in the first device, ~21.3 meV. (The $X_D^R - X_D$ energy splitting value is included in Supplementary Note 5 for all the four devices that we have measured.) From Fig. 3a, b, it is obvious that the spectrum weight of all the resolved excitonic complexes depends sensitively on the top gate voltage that effectively controls the density and type of charge carriers in the monolayer WSe₂. While the X⁺ occurs when the monolayer WSe₂ is hole-doped, X_1^-, X_2^-, and XX⁻ emerge when the WSe₂ is electron-doped, and XX only exists in the charge-neutral region[28,43,44,49]. It can be seen in Fig. 3a that the regions where X_D and X_D^R exist overlap significantly. For a quantitative understanding, we plot the integrated PL intensity as a function of the gate voltage for each excitonic complex in Fig. 3c. We find that the gate-voltage-dependent integrated PL intensity of the dark exciton replica exactly mimics that of the dark exciton, both reaching the maximum near the charge-neutral region and decreasing rapidly with either electron-doping or hole-doping (gate voltage > 0 V or< −2 V, as indicated by the onset of significant PL intensity from negative trions or positive trion). The charge-neutral region also strongly correlates with the PL intensity of the dark exciton. This

gate-voltage-dependent measurement rules out the possibility that the dark exciton replica is a charged dark exciton.

The gate-voltage-dependence and magnetic-field-and of the PL demonstrate that X_D and X_D^R are both charge-neutral excitations, and they should also share similar valley-spin configurations and wavefunctions. The sample-independent energy difference (~21.6 meV) between X_D and X_D^R and their sharp PL peaks further suggest that X_D^R, a previously unrecognized excitation of monolayer WSe₂, arises from coupling X_D to a quasiparticle at ~21.6 meV which cannot be a charge carrier or a plasmon. Based on these analyses, we attribute X_D^R to a phonon replica state formed by the coupling between X_D and a phonon. To check this assumption and identify the phonon mode involved, we first perform a first-principles calculation of the phonon dispersions of monolayer WSe₂. Our results show that doubly degenerate E″ phonon modes appear with vibration energy $\hbar\omega_{E''}$=21.8 meV, consistent with previous reports[24,50,51]. This energy is in excellent agreement with our observation of the $X_D - X_D^R$ energy difference of 21.6 meV.

Electron-phonon coupling in WSe₂. Despite the energy agreement, it is entirely unexpected that the phonon replica PL shows an intensity comparable to the bright exciton PL (Figs. 1b and 2b), which normally would require a strong exciton-phonon coupling strength or large phonon population. Furthermore, on closer examination of the optical spectra under magnetic fields (Figs. 1b and 2b), we find that the higher-energy replica peak is much stronger than the lower-energy one, meaning that the replica PL arising from each valley has finite circular polarization. For instance, at 5 T, we estimate the degree of circular polarization of the phonon replica to be 72% (See Supplementary Note 6). To understand these features, we first look into the spatial symmetry of the WSe₂ lattice in the presence of E″ phonons. In Fig. 4a (inset), we schematically plot one of the doubly degenerate E″ lattice vibrational modes that involve the opposite in-plane movement of the upper-plane and lower-plane Se atoms along x. This vibration breaks the mirror symmetry about the 2D plane and the threefold rotation symmetry. Furthermore, the vibration modes along the two in-plane directions can construct two chiral E″ phonon modes[50] at the gamma point, with angular momentum of 1 and −1, respectively. As a result, the excitons in the K or K' valleys can acquire a finite angular momentum and be brightened up by coupling to one of the chiral combinations (1 for K valley or −1 for K' valley) (see Supplementary Note 12). To illustrate this effect on the electrons quantitatively, we plot the conduction bands (Fig. 4a) and their in-plane spin components (S_x and S_y) at the K valley (Fig. 4b), in a structure with the upper-plane and lower-plane Se atoms displaced along x by 0.035 Å (i.e., zero-point motion amplitude) and −0.035 Å, respectively. At the K point, we obtain a conduction band splitting of 49 meV, 9 meV larger than that of 40 meV in the equilibrium structure. More significantly, S_x of the two conduction bands at K, initially 0 in the equilibrium structure, increases to $0.27\hbar$ and $-0.27\hbar$ after the displacement. Such band splitting enhancement and spin realignment clearly demonstrate an emerging in-plane spin-orbit field arising from the lattice vibrations (details and an analysis of the valence bands are included in Supplementary Note 11). As such, the E″ phonons are analogous to a fluctuating in-plane effective magnetic field that induces finite coupling between the two conduction bands and between the bright and dark excitons in the same valley[30], thus greatly enhancing out-of-plane and circularly polarized PL of X_D^R.

Perturbation theory of phonon-photon emission. We further use a frozen phonon method and a second-order perturbation
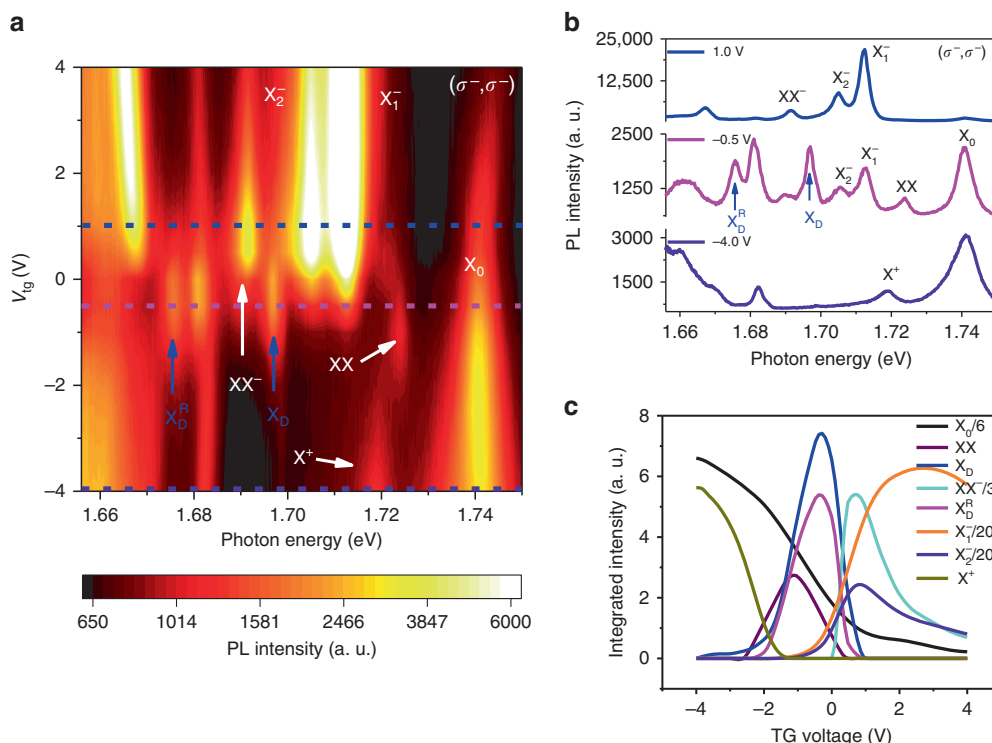
Fig. 3 Gate-dependent PL intensity of the dark-exciton and its replica. **a** PL spectra at 4.2 K as a function of the top gate voltage for a second BN encapsulated monolayer WSe_2 device. The color represents the PL intensity. The excitation is a CW laser centered at 1.959 eV with an excitation power of 40 μW, under which the biexciton (XX) and the charged biexciton (XX^-) are also visible. The gate dependence of the dark exciton replica X_D^R is similar to that of the dark exciton. **b** The line traces from (**a**) for the gate voltages of 1.0 V (blue), −1.0 V (magenta) and −4.0 V (purple). **c** Integrated PL intensity for different exciton complexes as a function of the gate voltage. The non-zero PL intensity regions for the dark exciton and its replica are almost identical, from ~−2.1 V to ~0.9 V of the top gate voltage
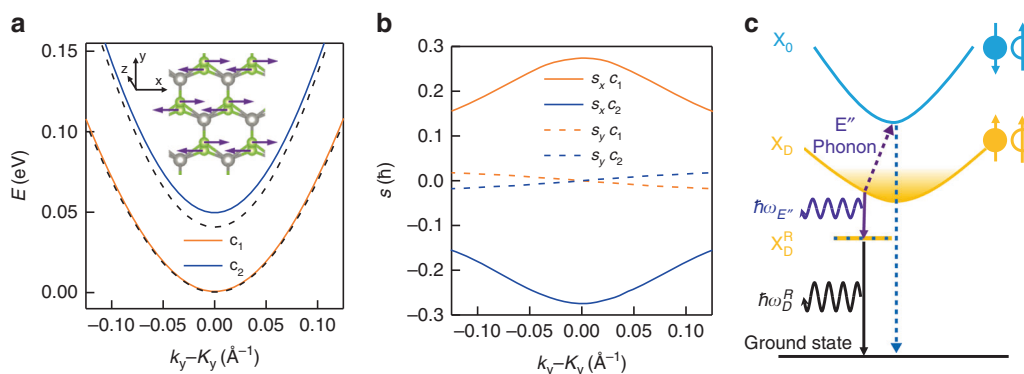
Fig. 4 Phonon coupling and recombination pathway of the K-valley dark-exciton. **a** The conduction band structure in the K valley, with the two Se atoms in one unit cell displaced by 0.035 and −0.035 Å, respectively, calculated using Kohn−Sham density functional theory. The conduction band bottom is set to 0 eV. The k path is taken along the y direction across the K point, i.e., $k_x = K_x$. The lower (c_1) and upper (c_2) conduction bands are colored orange and blue, respectively. The black dashed lines are the two conduction bands in the equilibrium structure. Inset: a schematic of an E'' phonon eigenmode. Gray and green spheres are W and Se atoms, respectively. Arrows indicate displacement. **b** Expectation values of conduction-band electron spin angular momentum in the x and y direction, S_x (solid line) and S_y (dashed line), of c_1 (orange) and c_2 (blue) as a function of k. **c** The bright exciton (X_O) band and dark exciton (X_D) band are denoted by the blue and yellow parabola, respectively. The solid circle and the empty circle represent the electron and the hole, respectively, while the arrows up and down indicate the spin orientation. The yellow-shaded area above X_D indicates a quasi-equilibrium population of dark excitons at 4.2 K. The dark-exciton phonon replica (X_D^R) state is labeled by a line with alternating blue and yellow color, indicating coupling between X_O and X_D by emitting a chiral E'' phonon of an energy $\hbar\omega_{E''}$ (purple wavy arrow). The photon emission by X_D^R is labeled by the black arrow, having an energy $\hbar\omega_D^R$. The emission process from X_D, in the second-order perturbation theory, is illustrated by the purple wavy and blue dashed lines, corresponding to the emission of a chiral E'' phonon and a circularly polarized photon, respectively. The intermediate state is the bright exciton X_O

theory (schematically shown in Fig. 4c) to calculate the photon emission probability of the phonon replica X_D^R relative to the bright exciton. The perturbing Hamiltonian consists of two terms, H_{ex-ph} and H_{ex-l}, arising from the exciton-phonon and exciton-

photon interactions, respectively. The exciton-phonon coupling allows the dark exciton to mix with the intravalley bright exciton by emitting a chiral E'' phonon; exciton-photon coupling describes circularly polarized light emission of the bright exciton

with an in-plane electric dipole (details in Supplementary Notes 10 and 12). The overall process, i.e., simultaneously emitting a chiral E'' phonon with an energy $\hbar\omega_{E''}$ and a circularly polarized photon with an energy $\hbar\omega_D^R$, have a transition probability given by the following equation,

$$W\left(\omega_D^R\right) = \left|\frac{\langle\Phi_D|H_{ex-ph}|\Phi_0\rangle\langle\Phi_0|H_{ex-l}|\Phi_G\rangle}{E_D - E_0 - \hbar\omega_{E''}}\right|^2 \delta\left(E_D - \hbar\omega_{E''} - \hbar\omega_D^R\right).$$

Here, Φ_D, Φ_0, and Φ_G are the wavefunctions of dark exciton, bright exciton, and ground state, respectively. At the experimental temperature of 4.2 K, the thermal energy of dark excitons are very small (~0.4 meV). We therefore use the zero-momentum dark exciton wavefunctions for Φ_D. In the equation, $|\langle\Phi_0|H_{ex-l}|\Phi_G\rangle|^2$ is the photon emission probability from the bright exciton. Therefore, the other term $\left|\frac{\langle\Phi_D|H_{ex-ph}|\Phi_0\rangle}{E_D-E_0-\hbar\omega_{E''}}\right|^2$, having a dimensionless value ~0.04, defines the ratio of photon emission probability between the replica state and the bright state (calculation details in Supplementary Notes 11 and 12). This large ratio, together with the long lifetime of dark excitons[30,31,52,53] of (~250 ± 20 ps in our device shown in Fig. 1, see Supplementary Fig. 7c), explains the significant replica PL in our experiment. It is worth noting that the dark exciton phonon replica possesses a lifetime of ~230 ± 20 ps, same as the dark exciton lifetime within the experimental uncertainty, confirming the phonon replica interpretation.

Discussion

The dark exciton state, owing to its distinctive symmetry properties, provides an intriguing way to directly probe the "dark" phonon mode. The exciton-phonon interaction, due to the unique symmetry of the E'' phonon mode, leads to the formation of the dark-exciton phonon replica which potentially inherits both long lifetime of dark exciton and valley polarization of the bright exciton. Our understanding sheds light on the manipulation of dark exciton through the new knob of lattice vibrations, which also furnishes a new route for dynamically manipulating the dark exciton through the phonon-exciton interactions.

Data availability

The data that support the findings of this study are available from the authors on reasonable request; see author contributions for specific data sets.

References

1. Cao, T. et al. Valley-selective circular dichroism of monolayer molybdenum disulphide. Nat. Commun. 3, 885–887 (2012).
2. Mak, K. F., He, K., Shan, J. & Heinz, T. F. Control of valley polarization in monolayer MoS_2 by optical helicity. Nat. Nanotechnol. 7, 494–498 (2012).
3. Zeng, H., Dai, J., Yao, W., Xiao, D. & Cui, X. Valley polarization in MoS_2 monolayers by optical pumping. Nat. Nanotechnol. 7, 490–493 (2012).
4. Xu, X., Yao, W., Xiao, D. & Heinz, T. F. Spin and pseudospins in layered transition metal dichalcogenides. Nat. Phys. 10, 343–350 (2014).
5. Wang, G. et al. Colloquium: excitons in atomically thin transition metal dichalcogenides. Rev. Mod. Phys. 90, 21001 (2018).
6. Wang, Z., Shan, J. & Mak, K. F. Valley- and spin-polarized Landau levels in monolayer WSe_2. Nat. Nanotechnol. 12, 144–149 (2016).
7. Jin, C. et al. Imaging of pure spin-valley diffusion current in WS_2-WSe_2 heterostructures. Science 360, 893–896 (2018).
8. Mak, K. F. & Shan, J. Photonics and optoelectronics of 2D semiconductor transition metal dichalcogenides. Nat. Photonics 10, 216–226 (2016).
9. Wang, K. et al. Electrical control of charged carriers and excitons in atomically thin materials. Nat. Nanotechnol. 13, 128–132 (2018).
10. Wang, Z., Mak, K. F. & Shan, J. Strongly interaction-enhanced valley magnetic response in monolayer WSe_2. Phys. Rev. Lett. 120, 066402 (2018).
11. Wang, F., Dukovic, G., Brus, L. E. & Heinz, T. F. The optical resonances in carbon nanotubes arise from excitons. Science 308, 838–841 (2005).
12. Ye, Z. et al. Probing excitonic dark states in single-layer tungsten disulphide. Nature 513, 214–218 (2014).
13. Chernikov, A. et al. Exciton binding energy and nonhydrogenic Rydberg series in monolayer WS_2. Phys. Rev. Lett. 113, 076802 (2014).
14. He, K. et al. Tightly bound excitons in monolayer WSe_2. Phys. Rev. Lett. 113, 026803 (2014).
15. Jones, A. M. et al. Optical generation of excitonic valley coherence in monolayer WSe_2. Nat. Nanotechnol. 8, 634–638 (2013).
16. Kylänpää, I. & Komsa, H. P. Binding energies of exciton complexes in transition metal dichalcogenide monolayers and effect of dielectric environment. Phys. Rev. B 92, 205418 (2015).
17. Kidd, D. W., Zhang, D. K. & Varga, K. Binding energies and structures of two-dimensional excitonic complexes in transition metal dichalcogenides. Phys. Rev. B 93, 125423 (2016).
18. Chen, C.-F. F. et al. Controlling inelastic light scattering quantum pathways in graphene. Nature 471, 617–620 (2011).
19. Ferrari, A. C. et al. Raman spectrum of graphene and graphene layers. Phys. Rev. Lett. 97, 187401 (2006).
20. Zhang, L. & Niu, Q. Chiral phonons at high-symmetry points in monolayer hexagonal lattices. Phys. Rev. Lett. 115, 115502 (2015).
21. Chow, C. M. et al. Phonon-assisted oscillatory exciton dynamics in monolayer $MoSe_2$. npj 2D Mater. Appl. 1, 33 (2017).
22. Kim, S., Kim, K., Lee, J. & Cheong, H. Excitonic resonance effects and Davydov splitting in circularly polarized Raman spectra of few-layer WSe_2. 2D Mater. 2, 045002 (2017).
23. Zhu, H. et al. Observation of chiral phonons. Science 359, 579–582 (2018).
24. Chen, X. et al. Entanglement of single-photons and chiral phonons in atomically thin WSe_2. Nat. Phys. 15, 221–228 (2018).
25. Luo, X. et al. Effects of lower symmetry and dimensionality on Raman spectra in two-dimensional WSe_2. Phys. Rev. B 88, 195313 (2013).
26. Chow, C. M. et al. Unusual exciton−phonon interactions at van der Waals engineered interfaces. Nano Lett. 17, 1194–1199 (2017).
27. Wang, L. et al. One-dimensional electrical contact to a two-dimensional material. Science 342, 614–617 (2013).
28. Li, Z. et al. Revealing the biexciton and trion-exciton complexes in BN encapsulated WSe_2. Nat. Commun. 9, 3719 (2018).
29. Meng, Y. et al. Excitonic complexes and emerging interlayer electron-phonon coupling in BN encapsulated monolayer semiconductor alloy: $WS_{0.6}Se_{1.4}$. Nano Lett. 19, 299–307 (2019).
30. Zhang, X. X. et al. Magnetic brightening and control of dark excitons in monolayer WSe_2. Nat. Nanotechnol. 12, 883–888 (2017).
31. Robert, C. et al. Fine structure and lifetime of dark excitons in transition metal dichalcogenide monolayers. Phys. Rev. B 96, 155423 (2017).
32. Zhou, Y. et al. Probing dark excitons in atomically thin semiconductors via near-field coupling to surface plasmon polaritons. Nat. Nanotechnol. 12, 856–860 (2017).
33. Wang, G. et al. In-plane propagation of light in transition metal dichalcogenide monolayers: optical selection rules. Phys. Rev. Lett. 119, 047401 (2017).
34. Zhang, X. X., You, Y., Zhao, S. Y. F. & Heinz, T. F. Experimental evidence for dark excitons in monolayer WSe_2. Phys. Rev. Lett. 115, 257403 (2015).
35. Xiao, D., Liu, G., Bin, Feng, W., Xu, X. & Yao, W. Coupled spin and valley physics in monolayers of MoS_2 and other group-VI dichalcogenides. Phys. Rev. Lett. 108, 196802 (2012).
36. Gong, Z. et al. Magnetoelectric effects and valley-controlled spin quantum gates in transition metal dichalcogenide bilayers. Nat. Commun. 4, 2053 (2013).
37. Ye, Z., Sun, D. & Heinz, T. F. Optical manipulation of valley pseudospin. Nat. Phys. 13, 26–29 (2017).
38. Plechinger, G. et al. Trion fine structure and coupled spin-valley dynamics in monolayer tungsten disulfide. Nat. Commun. 7, 12715 (2016).
39. Yu, H., Liu, G., Bin, Gong, P., Xu, X. & Yao, W. Dirac cones and Dirac saddle points of bright excitons in monolayer transition metal dichalcogenides. Nat. Commun. 5, 3876 (2014).
40. Jones, A. M. et al. Excitonic luminescence upconversion in a two-dimensional semiconductor. Nat. Phys. 12, 323–327 (2016).
41. Singh, A. et al. Long-lived valley polarization of intravalley trions in monolayer WSe_2. Phys. Rev. Lett. 117, 257402 (2016).
42. Steinhoff, A. et al. Biexciton fine structure in monolayer transition metal dichalcogenides. Nat. Phys. 14, 1199–1204 (2018).
43. Ye, Z. et al. Efficient generation of neutral and charged biexcitons in encapsulated WSe_2 monolayers. Nat. Commun. 9, 3718 (2018).

44. Barbone, M. et al. Charge-tuneable biexciton complexes in monolayer WSe$_2$. *Nat. Commun.* **9**, 3721 (2018).
45. Aivazian, G. et al. Magnetic control of valley pseudospin in monolayer WSe$_2$. *Nat. Phys.* **11**, 148–152 (2015).
46. Macneill, D. et al. Breaking of valley degeneracy by magnetic field in monolayer MoSe$_2$. *Phys. Rev. Lett.* **114**, 037401 (2015).
47. Srivastava, A. et al. Valley Zeeman effect in elementary optical excitations of monolayer WSe$_2$. *Nat. Phys.* **11**, 141–147 (2015).
48. Li, Y. et al. Valley splitting and polarization by the Zeeman effect in monolayer MoSe$_2$. *Phys. Rev. Lett.* **113**, 266804 (2014).
49. Chen, S.-Y., Goldstein, T., Taniguchi, T., Watanabe, K. & Yan, J. Coulomb-bound four- and five-particle intervalley states in an atomically-thin semiconductor. *Nat. Commun.* **9**, 3717 (2018).
50. Shin, D. et al. Phonon-driven spin-Floquet magneto-valleytronics in MoS$_2$. *Nat. Commun.* **9**, 638 (2018).
51. Mishra, H., Bose, A., Dhar, A. & Bhattacharya, S. Exciton−phonon coupling and band-gap renormalization in monolayer WSe$_2$. *Phys. Rev. B* **98**, 045143 (2018).
52. Nagler, P. et al. Zeeman splitting and inverted polarization of biexciton emission in monolayer WS$_2$. *Phys. Rev. Lett.* **121**, 57402 (2018).
53. Robert, C. et al. Exciton radiative lifetime in transition metal dichalcogenide monolayers. *Phys. Rev. B* **93**, 205423 (2016).

Author contributions

S.-F.S. conceived the experiment. Z. Li, Y.M. and Z. Lian fabricated the devices. Z. Li, T.W. and Z. Lu performed the measurements. S.-F.S., Z. Li, T.W., C.J., T.C. and Z. Lian analyzed the data. C.J. and T.C. performed calculations of the exciton−phonon coupling and developed a theoretical framework that interprets the replica photoluminescence. L.Y. and S.G. performed DFPT calculation of the phonon modes. T.R. contributed to the discussion. T.T. and K.W. grew the BN crystals. S.T. and M.B. grew defect-free WSe$_2$ crystals using a modified flux growth method. S.-F.S. supervised the project. D.S. supervised the magneto-PL measurements. S.-F.S. and T.C. wrote the manuscript with the input from all the other co-authors. All authors discussed the results and contributed to the manuscript.

Additional information

Supplementary Information accompanies this paper at https://doi.org/10.1038/s41467-019-10477-6.

Competing interests: The authors declare no competing interests.

Reprints and permission information is available online at http://npg.nature.com/reprintsandpermissions/

Journal peer review information: *Nature Communications* thanks Fanyao Qu and other anonymous reviewer(s) for their contribution to the peer review of this work.

Publisher's note: Springer Nature remains neutral with regard to jurisdictional claims in published maps and institutional affiliations.